EXOSUITS

Effect of hip abduction assistance on metabolic cost and balance during human walking

Juneil Park[1], Kimoon Nam[1], Juseok Yun[1,2], JunYoung Moon[1], JaeWook Ryu[1], Sungjin Park[1], Seungtae Yang[1,2], Alireza Nasirzadeh[1], Woochul Nam[1], Sruthi Ramadurai[3], Myunghee Kim[3]*, Giuk Lee[1]*

The use of wearable robots to provide walking assistance has rapidly grown over the past decade, with notable advances made in robot design and control methods toward reducing physical effort while performing an activity. The reduction in walking effort has mainly been achieved by assisting forward progression in the sagittal plane. Human gait, however, is a complex movement that combines motions in three planes, not only the sagittal but also the transverse and frontal planes. In the frontal plane, the hip joint plays a key role in gait, including balance. However, wearable robots targeting this motion have rarely been investigated. In this study, we developed a hip abduction assistance wearable robot by formulating the hypothesis that assistance that mimics the biological hip abduction moment or power could reduce the metabolic cost of walking and affect the dynamic balance. We found that hip abduction assistance with a biological moment second peak mimic profile reduced the metabolic cost of walking by 11.6% compared with the normal walking condition. The assistance also influenced balance-related parameters, including the margin of stability. Hip abduction assistance influenced the center-of-mass movement in the mediolateral direction. When the robot assistance was applied as the center of mass moved toward the opposite leg, the assistance replaced some of the efforts that would have otherwise been provided by the human. This indicates that hip abduction assistance can reduce physical effort during human walking while influencing balance.

INTRODUCTION

Walking is an essential activity in our daily lives. Humans walk about 5000 steps and cover a distance of 2.5 miles (4 km) per day, which typically takes around 80 min (*1*–*4*). Among nonexercise activities, humans spend the most energy on walking (*5*). This has captured the attention of researchers to explore gait-assistive robots that can improve walking ability, especially from an energy-efficiency perspective (*6*). Starting with the study by Malcolm *et al.* (*7*), notable advancements in robot design and control methods have enabled a reduction in human effort while performing an activity (*7*–*18*), including a 50% metabolic cost reduction when walking at a range of walking speeds compared with the exoskeleton-unpowered condition (*19*). This reduction was mainly accomplished by assisting fore-aft motion for forward progression (*7*–*15*). Previous studies have shown that push-off accomplished by facilitating forward progression in the fore-aft direction, mostly explained in the sagittal plane, can also influence frontal plane motion (*20*, *21*); similarly, assistance along the frontal plane may influence forward progression and physical effort. However, there has been limited research to date exploring the effects of frontal plane assistance on the physical effort of walking.

The frontal plane motion can be understood as a balance-restoring method, such as adjusting the foot placement via hip abduction and adduction (*22*, *23*) or restraining the pelvic drop because of sudden loading when the contralateral limb transits from the stance phase to the swing phase (*24*). In terms of gait, the primary function of hip abduction is to prevent the pelvis from dropping because of gravitational force when one foot is lifted off the ground. On the other hand, hip adduction contributes to the lateral movement of the hip during gait by assisting hip extension (*24*). When performing this functional role, hip ab/adduction presents the highest torque and peak power among the motions in the frontal plane (*25*). In addition, among the three planes of the lower extremity joints comprising nine combinations, this torque and power are the third largest, after those due to ankle plantar flexion/dorsiflexion and hip extension/flexion in the sagittal plane (*25*), suggesting that hip ab/adduction assistance can also influence walking energetics.

In a simulation study, Dembia *et al.* (*26*) investigated the effects of hip abduction assistance on the metabolic cost of loaded walking and found that this assistance was sufficient to reduce the physical effort of walking. In particular, the study found that hip abduction assistance could provide the greatest ratio of reduced metabolic rate to the peak instantaneous positive device power. During walking, the hip joint in the frontal plane presents a strong abductor pattern, with two peaks at the moment and two positive peaks in power (*25*). In other words, the hip abductor is mainly responsible for energy generation/absorption in the frontal plane. If a robot provides torque in a timely manner, then it can substitute a portion of the physical effort of walking that was originally required of a human (*8*, *9*, *11*, *27*). Hip abduction assistance, therefore, may reduce the metabolic cost of human walking.

Because hip ab/adduction plays a key role in gait, a few attempts have been made to assist frontal plane motion. Zhang *et al.* (*28*) developed a hip exoskeleton that can assist both fore-aft and mediolateral motions. The system integrated the center of mass (CoM) concept into the admittance controller to assist the hip in the

[1]School of Mechanical Engineering, Chung-Ang University, 06974 Seoul, South Korea. [2]HUROTICS Inc., 06974 Seoul, South Korea. [3]Mechanical and Industrial Engineering, University of Illinois Chicago, Chicago, IL, USA.
*Corresponding author. Email: myheekim@uic.edu (M.K.); giuklee@cau.ac.kr (G.L.)

frontal plane, broaden the step width, and improve lateral stability. The authors evaluated the system performance by conducting a human participant experiment with three participants whose speeds ranged from 0.45 to 0.65 m s^{-1}. The results suggested that assistance in both the fore-aft and mediolateral directions could potentially be provided, thus influencing stability at slow speeds. A controlled human participant experiment with a greater number of participants is required to further validate the effects of assistance on balance. Chiu *et al.* (*29*) also developed a device to assist both the sagittal and frontal planes simultaneously and assessed the system performance. The effects of Chiu *et al.*'s system on walking have not yet been analyzed. Yang *et al.* (*30*) designed a soft wearable robot for hip abductor assistance. They implemented force profiles based on the simulation study by Dembia *et al.* (*26*). The authors found that the robot reduced the peak knee adduction moment and the impulse of the knee adduction moment for eight participants by increasing hip abduction and shifting the body's CoM laterally. From these results, we ascertained that hip abduction assistance can influence the mechanics of the CoM in the mediolateral direction and that a specific assistive method may help reduce energy consumption or improve dynamic balance during walking.

Prior experimental and simulation studies have suggested that hip assistance in the frontal plane has the potential to reduce the physical effort of walking and influence balance. Here, we aimed to evaluate and understand the effect of hip abduction assistance during walking. We hypothesized that hip abduction assistance with a peak timing from biological hip abduction torque or power would decrease the metabolic cost of walking by replacing a portion of the human effort. To test this hypothesis, we developed a soft hip exosuit with hip ab/adduction assistance and altered the assistance profiles in time while maintaining the magnitude of the force and duration of assistance (*8*, *9*). We set four different assistance profiles for hip abduction, mimicking the biological properties of the hip joint in the frontal plane (Fig. 1), and designed the peak timing of the assistance profiles to coincide with the biological peak timings. These are referred to as the moment first peak mimic profile (MF), power first peak MF (PF), moment second peak MF (MS), and power second peak MF (PS). We expected that the human responses would be different depending on the profiles, given that the biological peaks appeared at different timings. The experiments were conducted using the tethered assistance system for hip abduction assistance. The experimental setup and protocol are represented in Fig. 2.

In terms of gait balance, through a simple dynamic walking model, Kuo *et al.* revealed that gait can be laterally unstable and that foot placement control can be an efficient and effective method to restore balance (*31*, *32*). When an external perturbation or stabilizer is present, people compromise their balance strategies. Hip abduction thus becomes involved in their strategies for maintaining balance (*34*, *35*). We thus speculated that gait balance can be influenced by hip abduction assistance, with the aim of reducing metabolic rate. Therefore, we hypothesized that strategies for maintaining gait balance would be influenced by the timing of hip abduction assistance. Dynamic gait balance is typically controlled by adjusting foot placement (*22*, *36*, *37*) or changing the step width or cadence (*22*, *38*–*40*). Changes in balance are represented as changes in the margin of stability (MoS) (*36*), variability in the center of pressure (CoP) (*41*), or changes in whole-body angular momentum (*42*–*44*). We measured the indicators related to dynamic gait balance, such as the lateral MoS, average step width and variability, stride length, cadence, and variability of the CoP. Detailed descriptions of these parameters are outlined in the Materials and Methods section and Movie 1.

RESULTS

Exosuit performance

The designed and measured control parameters are summarized in Fig. 3 and Table 1. The designed control parameters are the peak force and peak timing, denoted by the units newton and gait cycle percentage, respectively. The measured control parameters were collected from the recorded data in this experiment. The peak force, peak timing, and average positive mechanical power in the measured parameters are represented as averages and SDs.

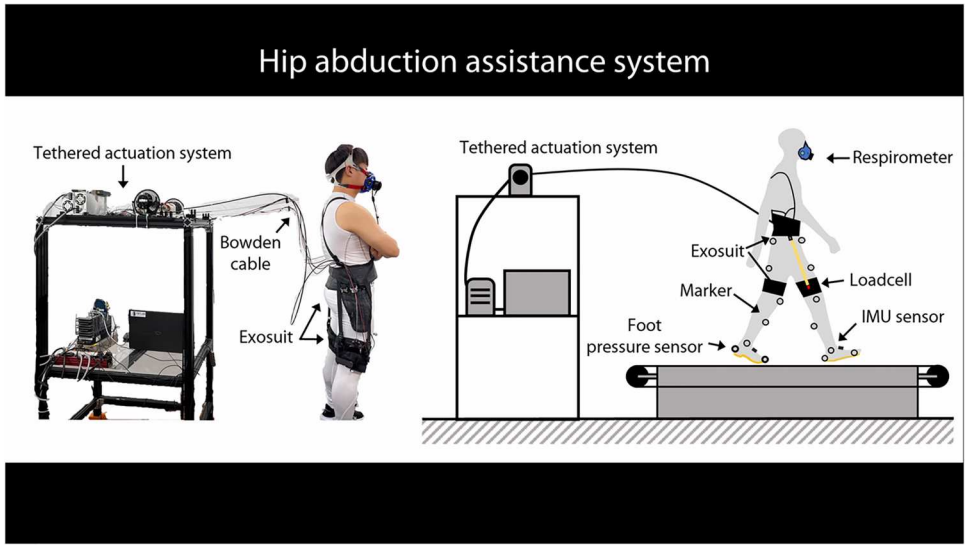

Movie 1. Overview of the hip abduction assistance system and its experimental results.

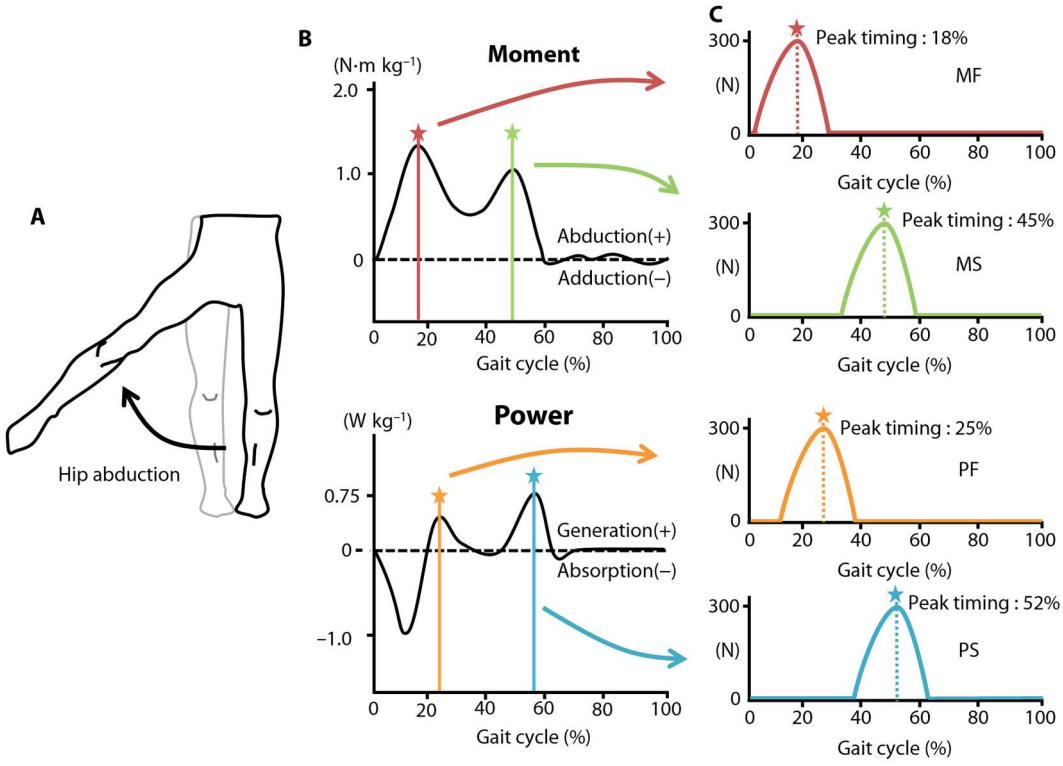

Fig. 1. Biological moment and power profile of the hip in the frontal plane. (**A**) Schematic of hip abduction in the standing posture. Hip abduction is the movement of the leg away from the body center. (**B**) General biological hip moment and power in the frontal plane. The positive and negative values in the moment profile indicate hip abduction and hip adduction moments, respectively. The hip moment mainly comprises the abduction moment. When the joint power becomes positive, energy is generated; when it becomes negative, energy is absorbed. Energy generation and absorption of the hip joint in the frontal plane appear with hip abduction. (**C**) Designed assistance profiles mimicking the biological characteristics of the hip joint moment and power. The profile was designed such that its peak coincides with the biological peaks. For example, the MF is a profile that mimics the first peaks of the hip abduction moment. The designed peak timings are denoted by the stars and dotted lines in each profile.

The peak force error and peak timing error are the differences between the measured outcome and the designed parameter and are denoted by the units newton and gait cycle percentage, respectively. These parameters were calculated by comparing the mean of the measured outcome of all the participants and their desired value. The hip abduction assistance system delivered the force with less than 1% gait cycle of the peak time error in all the powered conditions. The peak force error was less than −32.31 N in the powered conditions, which was equal to the 10.77% error rate of the peak force. The delivered mechanical power over the stride is represented in Fig. 3, and the average positive power is shown in Table 1. The mechanical power delivered by the soft exosuit was calculated by multiplying the force recorded by the load cell, moment arm, and angular velocity of the thigh.

Metabolic cost

The assistance timing significantly affected the metabolic cost of walking [analysis of variance (ANOVA), $P = 1.03 \times 10^{-4}$] (Fig. 4). Compared with the normal walking condition (walking without the hip abduction assistance exosuit), the MS condition mimicking the rear peak of the biological moment statistically significantly reduced the metabolic cost of walking by −11.36 ± 10.16% (paired t test, P = 0.009). The average change in metabolic rate for the MF, PF, and PS conditions was 6.95 ± 9.93%, 1.93 ± 14.3%, and 6.68 ± 11.06%, respectively.

Balance-related parameters

The assistive timing statistically significantly influenced the MoS in the mediolateral direction (ANOVA, $P = 1.76 \times 10^{-4}$) (Fig. 5A). All of the powered conditions (MF, MS, PF, and PS conditions) had a lower MoS in the mediolateral direction (MoS ML) compared with the normal walking condition. In the PS condition, the MoS ML was significantly lower compared with the MF and MS conditions (P = 0.007 and $P = 6.7 \times 10^{-5}$, respectively); however, it did not show a statistical difference with the PF condition (P = 0.075).

The assistive timing statistically significantly influenced the step width variability (Friedman, $P = 6.55 \times 10^{-4}$) (Fig. 5A). The normal walking condition had the lower step width variability compared with the MS condition (Dunn-Bonferroni test, P = 0.007). The other powered condition also tended to have a larger step width variability compared with the normal walking condition (Fig. 5A and table S3). The step width variability for the MF condition was significantly different compared with the other powered conditions (Dunn-Bonferroni test, $P \leq 0.009$). The variability of the CoP and the average step width did not show any statistical difference (Friedman, P = 0.177 and P = 0.131, respectively).

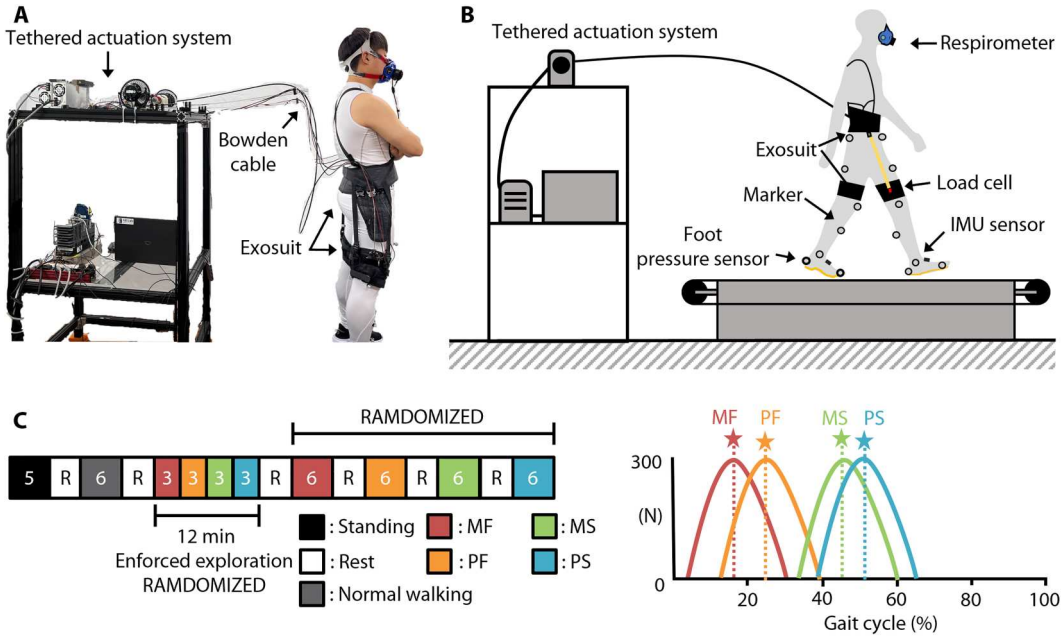

Fig. 2. Experimental setup and protocol. (**A**) Photograph of the experimental setup. Participants wore an exosuit providing hip abduction assistance. The experiment was conducted on a treadmill. (**B**) Schematic of the experimental setup. The tethered actuation system was situated behind the participants, delivering the actuation force using a cable. The sensors and devices, including the respirometer, markers, foot pressure sensor, load cells, and IMU sensors, were attached to the participants to record various biological changes during the experiment. (**C**) The experimental protocol. All walking trials lasted 6 min. After the standing and normal walking conditions, the participants went through an enforced exploration period for a total of 12 min, during which robot assistance was applied while the participants walked in the instructed posture. The participants tried to adapt to the assistance offered by the robot. The main test session was conducted after the enforced exploration session. The order of powered conditions of the main test and enforced exploration session was randomized, and the participants rested at least 5 min between walking trials.

Spatiotemporal parameters

The assistive timing also influenced the spatiotemporal parameters (Fig. 5C). The stride length (ANOVA, P = 0.016), cadence (ANOVA, P = 0.014), stance time (ANOVA, P = 0.002), and double stance time (ANOVA, $P = 2.19 \times 10^{-4}$) changed statistically significantly across all the conditions. Compared with the normal walking condition, the stride length for the MS condition was reduced by 1.96% (paired t test, P = 0.003). In the MS condition, the stride length statistically differed from the MF and PF conditions (paired t test, P = 0.024 and P = 0.020, respectively); however, it was not statistically different compared to the PS condition (paired t test, P = 0.999). The cadence tended to increase in the MS and PS conditions (1.65 and 1.18%, respectively) and reduce in the MF and PF conditions compared with the normal walking condition (−1.88 and −0.6%, respectively). The MS condition increased cadence by more than 0.46% compared with the MF (P = 0.008), PF (P = 0.004), normal walking (P = 0.001), and PS conditions (P = 0.993). The stance time and double stance time showed a similar trend. Both were relatively shorter in the MS and PS, although they were longer in the MF and PF compared with the normal condition. In particular, the double stance time was reduced in the MS condition by 4.93% compared with the normal walking condition (paired t test, P = 0.002). The swing time did not show a statistical difference (ANOVA, P = 0.217).

Kinematics of CoM

The position, velocity, and acceleration of the CoM in the mediolateral direction are depicted in Fig. 6. We defined the CoM as the midpoint of the posterior superior iliac spine markers. The position, velocity, and acceleration of the CoM in the mediolateral direction were time-normalized by the gait cycles starting from the right heel strike (RHS) and then averaged across the participants. The

Table 1. Exosuit performance parameters. Designed and measured control parameters in the powered conditions.

	Designed		Measured				
	Peak force (N)	Peak timing (% gait cycle)	Peak force (N)	Peak timing (% gait cycle)	Average positive mechanical power (W kg^{-1})	Peak force error (N)	Peak timing error (% gait cycle)
MF	300	17	281.3 ± 12.0	17.3 ± 0.8	0.132 ± 0.053	−9.82	0.66
PF	300	25	280.2 ± 8.7	25.7 ± 0.7	0.219 ± 0.051	−16.91	0.68
MS	300	45		45.5 ± 0.9	0.244 ± 0.084	−21.91	0.82

continued on next page

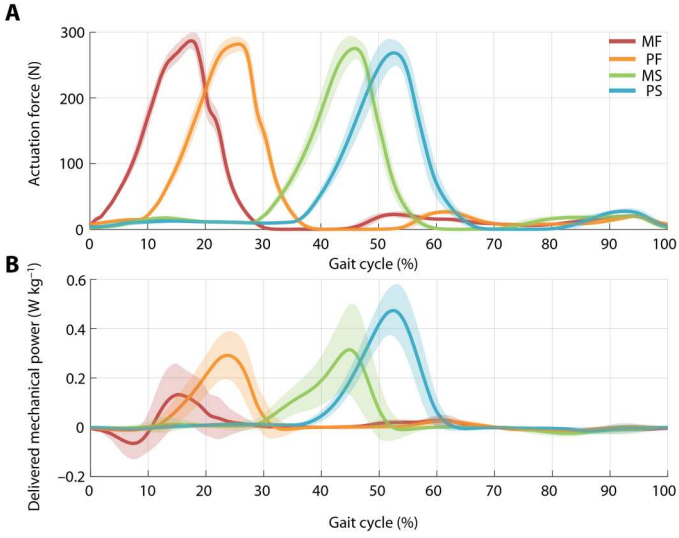

Fig. 3. Assistance profiles and delivered mechanical power. (**A**) Assistance force profiles over the gait cycles for each condition averaged across the participants. The solid line represents the average force, and the shaded areas represent ± 1 SD. The assistance profiles were designed to have the same peak force and duration. (**B**) Delivered mechanical power normalized to the body mass. The solid line represents the average mechanical power, and the shaded areas represent ± 1 SD. The delivered mechanical power was calculated by multiplying the moment and angular velocity of the thigh, organized over the gait cycle for each condition and averaged across the participants. MF, PF, MS, and PS are denoted in red, yellow, green, and blue lines, respectively.

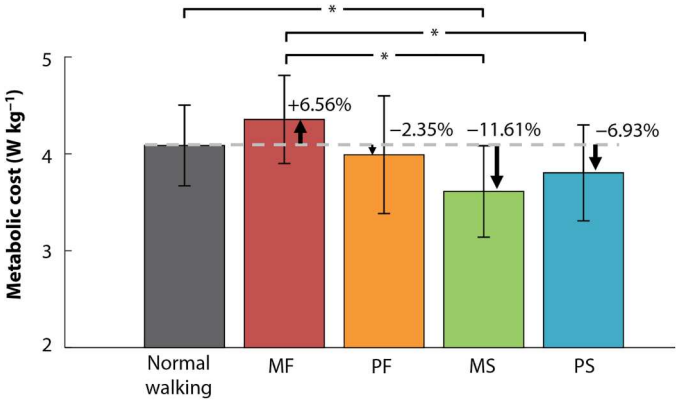

Fig. 4. Metabolic cost. Metabolic cost (W kg^{-1}) of the normal walking and four-powered conditions for all participants (n = 10). The error bars indicate the SD of the metabolic rate of all the participants in each condition. The asterisk represents the statistical significance (P < 0.05).

maximum position of CoM in the stance phase (the most lateral position) was statistically significantly influenced across all the conditions (ANOVA, P = 0.005). The acceleration of the CoM tended to increase toward the opposite leg when the hip abduction assistance was applied (Fig. 6D).

DISCUSSION

We designed a robot system to assist hip abduction and evaluated human responses when assistance was applied. After only a single day of training, we found that the profile mimicking the hip MS reduced the metabolic cost of human walking by 11.61% compared with the normal condition and provided positive mechanical power (Fig. 3). The metabolic cost reduction was similar to the level reported by the simulation study with an ideal actuator (about 12.9%) of Dembia *et al.* (*26*). The ideal actuation profile for the hip abduction assistance from the simulation study comprised large peak moments, including the peak located near the second peak timing of the biological moment. Similarly, our study also found that the profile, in our case the MS, showed a great metabolic cost reduction.

Instead of multiple days of an experimental protocol, having the training and test day separately, we observed the metabolic cost reduction after a 1-day protocol with five novice and five experienced participants. It appeared that hip abduction usage was relatively intuitive for the participants, thus reducing the metabolic cost of walking. To further help the participants use the hip abduction assistance, we introduced enforced exploration, a training method containing verbal instructions to explore several gait patterns as robot assistance was applied. They sought a proper strategy to walk with robot assistance. This effort could consequently have contributed to the participants using the robot assistance more efficiently (*45*) in a short time frame (3 min for each profile). Additional training days or training protocols (*46*) might have reduced the metabolic cost of walking even further.

Among the powered conditions, only the MS condition showed a statistically significant reduction in metabolic cost (−11.61%, P = 0.009), although the PF and PS conditions showed a lower reduction in metabolic cost on average compared with the normal walking condition (−2.35 and −6.93%, respectively). In general, a greater reduction in metabolic cost was demonstrated, provided that a wearable robot delivers more positive mechanical power (*9*, *47*–*49*). For the PS condition, it appeared that even if participants received the highest average positive power (Fig. 3, Table 1, and fig. S1), they spent balance-related effort when using the assistance. The PS had the lowest MoS and the highest step width variability compared with the other profiles (Fig. 5). Assistance in the PS was located around the end of the stance phase, and the force remained after the toe-off event (Fig. 3). We posited that the remaining force could drag the swing leg sideways, threatening the posture and increasing gait variability. Therefore, balance-related efforts were needed to have the participants walking steadily, resulting in the PS contributing to a lower reduction in metabolic rate than the MS.

The free-body diagram of the hip abduction assistance is depicted in Fig 7. When the actuator pulled the Bowden cable, an external force was applied to the contact leg, which generated an abduction moment at the hip joint center ($\boldsymbol{M}_{robot}$). Because the robot assistance was applied in the stance phase (Fig. 3), the external moment from the hip abduction assistance enhanced the movement of the stance leg, pushing the ground in a medial direction (Fig. 7). The reaction force acting opposite to the force pushing against the ground affected the foot in the medial direction (x axis, F_x), causing an external acceleration toward the contralateral leg on the CoM. The external accelerations due to hip abduction assistance are indicated in Fig. 6D. The acceleration of the CoM tended to be greater toward the opposite leg. The solid-colored line of each powered condition is also shown in Fig 6D. The results suggest that hip abduction assistance added shear force to the CoM.

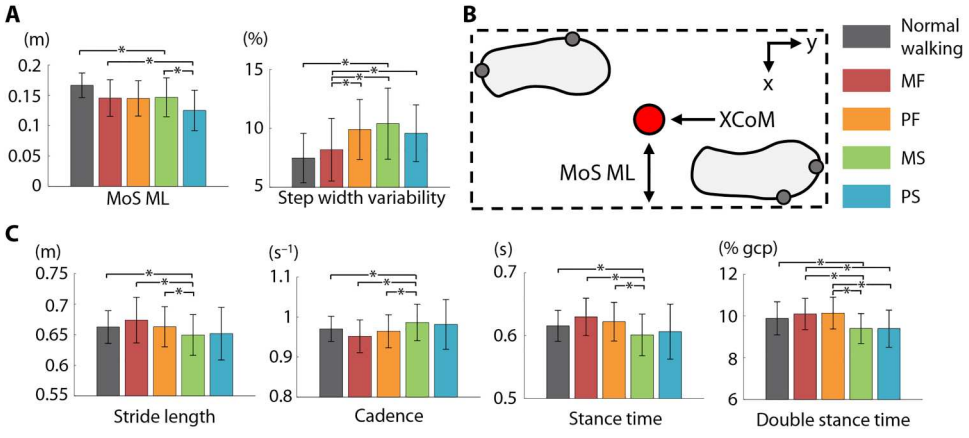

Fig. 5. Balance-related and spatiotemporal parameters. (**A**) Balance-related parameters. The MoS ML is calculated as the minimum distance between the BoS and the XCoM. The step width variability is represented in the form of the CV, which is normalized by its average. The MoS ML and step width variability were changed depending on the conditions (ANOVA, $P = 1.76\ 10^{-4}$; Friedman, $P = 6.55\ 10^{-4}$). (**B**) Gray circles on each foot form the boundary at the BoS. The red circle indicates the XCoM. (**C**) Spatiotemporal parameters. The stride length is defined as the distance between two feet in the anterior-posterior direction at the moment of HS. Cadence is defined as the reciprocal of stride time, and stance time is the time between one foot being placed on the ground and the time taken to fall. Double stance time is the time when both feet are on the ground simultaneously, represented as the gait cycle percentage normalized by the stride time. The bars and error bars denote the average and SD, respectively. The asterisk symbols indicate statistical significance ($P < 0.05$).

The hip abduction assistance can influence the kinematics of the CoM. Figure 6A shows the trajectory of the CoM from the top view. When the gait cycle started, the CoM moved toward the lateral position of the stance leg. Once the CoM reached the most lateral position, indicated by the red arrow, the CoM moved toward the opposite leg. On the basis of the most lateral position of the CoM, the assistance profile can be divided into two groups: the MF and PF, with the peak of the assistance profile appearing before the CoM reaches the most lateral position, and the MS and PS, with the peak of the assistance profile appearing after the CoM reaches the most lateral position. Figure 6D shows the acceleration of the CoM in the mediolateral direction. The powered conditions had a greater magnitude of acceleration in the contralateral direction, meaning that the hip abduction assistance accelerated the CoM toward the opposite leg. From the single stance phase, the velocity of CoM decelerated until the CoM reached the most lateral position. After reaching the most lateral CoM position, the CoM accelerated toward the opposite leg. The second group, MS and PS, tended to show reduced metabolic rates compared with the normal walking condition (−11.61 and −6.93%, respectively); however, the first group, MF and PF, showed a higher or statistically not different metabolic rate compared with the normal walking condition (Fig. 4). We posited that by applying hip abduction assistance at the moment the body's CoM naturally begins to shift toward the opposite leg, the assistance could reduce the physical effort required for walking. By synchronizing the assistance with this natural movement, the device could assume some of the workload typically exerted by the user, thereby lowering their energy expenditure or metabolic rate. However, when the hip abduction assistance was applied in the region wherein the velocity of the CoM was naturally directed toward the ipsilateral leg, it might have decelerated the CoM, but a reduction in metabolic rate can be challenging. From this perspective, the MS and PS reduced the metabolic rate by helping transfer the CoM toward the contralateral leg, but the MF and PF might aggravate and barely affect the energy consumption during walking because they provided assistance when the CoM decelerated.

The effects of acceleration toward the contralateral direction are shown by changes in the spatiotemporal parameters. We compared the maximal lateral position of each condition and found that there were statistical differences on the basis of the assistance timing. The result suggests that the CoM tended to move more laterally when the hip abduction assistance was applied (ANOVA, $P = 0.005$) (Fig. 6B). The maximal lateral position was calculated as the most lateral position of the average trajectory of the CoM of all the participants. The MS and PS, profiles that might help the CoM accelerate toward the contralateral direction, had a shorter stance time (Fig. 5C). Because the profiles were applied in the late stance phase (Fig. 3), the double stance time of the MS and PS conditions was also shorter compared with the other conditions (Fig. 5C). Conversely, the MF and PF conditions had a longer stance time. Perhaps, because the assistance was applied before the CoM reached its most lateral position, the assistance could have influenced the CoM to move more laterally and barely helped the CoM move toward the opposite leg, meaning participants had a longer stance time until the CoM was completely transmitted to the contralateral leg. The swing time, however, did not change statistically significantly (ANOVA, $P = 0.217$). Therefore, the stride time showed a similar trend to the stance time. Cadence, defined as the reciprocal of stride time, showed a trend opposite to the stance time. The cadence and stride length in this study revealed opposite trends. This is because the participants walked on a treadmill at a constant speed. Comprehensively, in the MS and PS conditions, where the metabolic benefits were seen, the participants tended to walk with shorter stride time and faster cadence.

As we hypothesized, hip abduction assistance led to changes in the balance-related parameters. The powered conditions showed a lower MoS ML, and the MoS ML in the PS was even lower compared with the other powered conditions. Several studies have revealed that the minimum MoS occurs after the heel strike (HS) (*50*, *51*). In this study, the MoS ML also appeared around when 10% of the

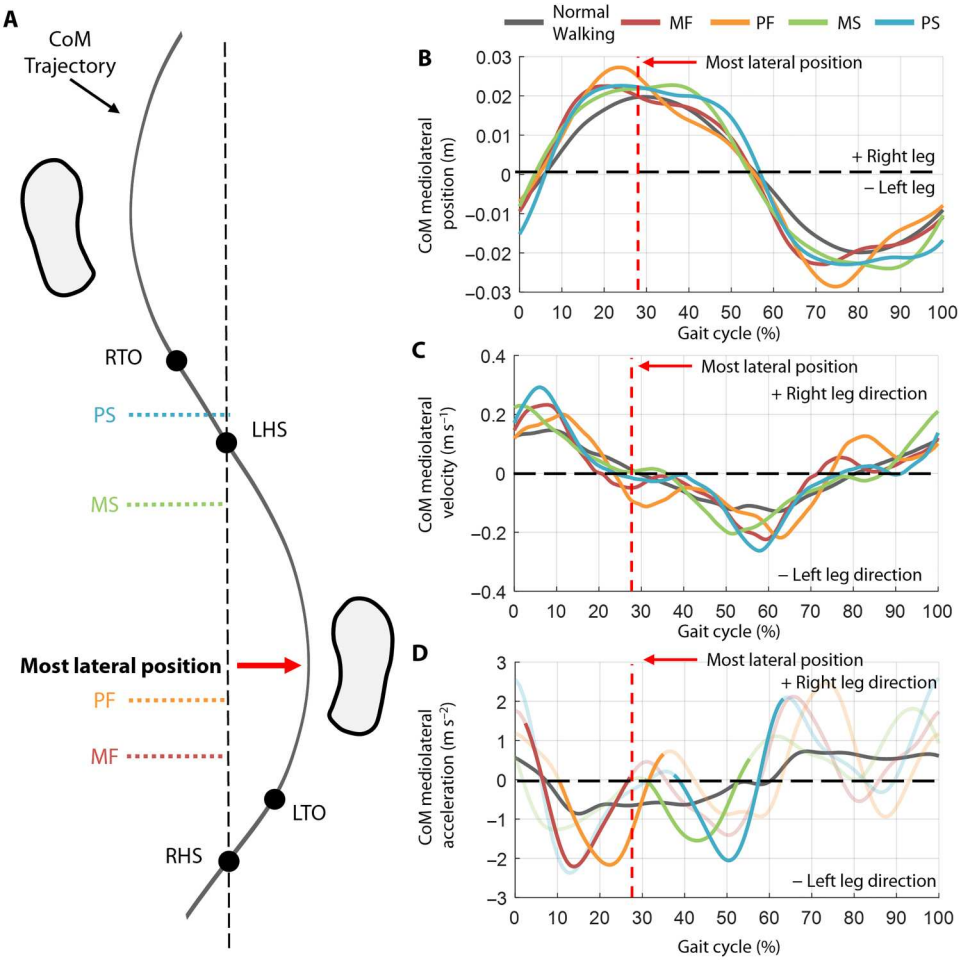

Fig. 6. CoM trajectory, mediolateral position, velocity, and acceleration. (**A**) Trajectory of the CoM from the top view. The solid gray line indicates the trajectory of the CoM. The red arrow indicates the most lateral position of the CoM in the stance phase. Each peak timing of the assistance profile is shown as a dotted, colored line. (**B** to **D**) Position, velocity, and acceleration of the CoM in the mediolateral direction, respectively. The position, velocity, and acceleration of the CoM in the mediolateral direction are represented by the gait cycles starting from the RHS averaged across the participants. The most lateral position of the CoM is also located in each plot. The hip abduction assistance tended to move the CoM laterally (ANOVA, $P = 0.005$). (**D**) The colored line indicates the acceleration of CoM in the mediolateral direction. The region in which robot assistance is applied is represented as a solid line. The hip abduction assistance accelerates the CoM in the contralateral direction (to the left leg in this figure).

gait cycle had been completed (fig. S2). At the time, the extrapolated CoM (XCoM) tended to be much higher (more lateral) in the MS and PS than in the other profiles. Because the assistance of MS and PS was provided in the late stance, it remained after the HS event of the ipsilateral leg in the opposite limb. We posited that because the assistance facilitated the CoM to move toward the opposite leg direction, XCoM became more lateral, and the MoS ML became lower when the assistance of the opposite limb remained (fig. S2). In many studies, a low MoS contributed to a loss of balance. In this study, it was observed that the powered conditions were relatively unstable compared with the normal walking condition. In the perturbation study conducted by Vlutter *et al.* (*35*), the authors suggested that when external perturbation existed, the hip abduction moment increased and the foot placement became more lateral. They also indicated that because both the planes (sagittal and frontal planes) are linked, a paired change in the sagittal and frontal planes occurs. For example, in a perturbation situation, the steps become wider and of shorter lengths simultaneously (*35*). We also noticed that step width and its variability tended to decrease when the lateral stability was improved (*34*). The coefficient of variation, CV, was affected by the assistance timing (Friedman, $P = 6.55 \times 10^{-4}$). In particular, the powered conditions tended to induce wider step width and higher variability (Fig. 5 and table S3).

Wang and Srinivasan (*33*) suggested that hip position and hip velocity, which approximates a body's CoM state, play an important role in determining foot placement during walking. In their research, the authors estimated that the next foot placement became wider (mediolateral) and shorter (fore-aft) through the more lateral position of the CoM state. In our research, we found that the CoM tended to move more laterally and that the average step width became wider, with the stride length becoming shorter with the application of hip abduction assistance (Figs. 5 and 6B and table S3). This result suggests that hip abduction assistance influences the foot

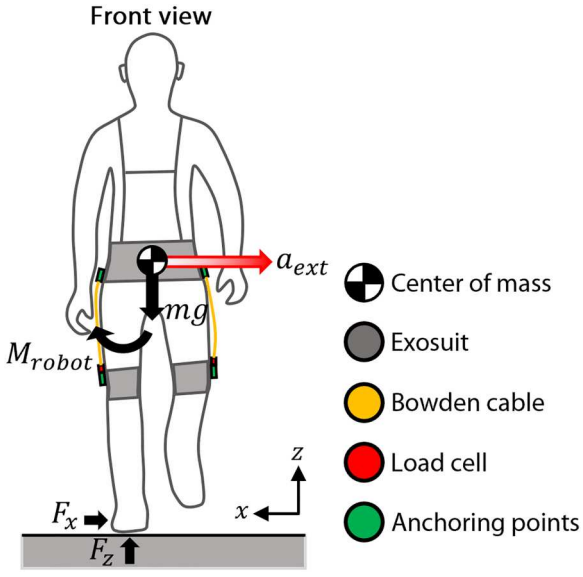

Fig. 7. Free-body diagram of the hip abduction assistance. When the actuator pulls the Bowden cable, the force generates an abduction moment on the hip joint ($\boldsymbol{M}_{\text{robot}}$). This moment adds additional shear force to the ground, after which reaction force is applied to the foot. Therefore, a resultant acceleration at the CoM toward the contralateral direction occurs ($\boldsymbol{a}_{\text{ext}}$).

placement strategy during walking. The changes in the CoM position confirmed these influences.

On the basis of the aforementioned studies, we postulated that hip abduction assistance may exacerbate gait stability. People spend more energy when gait balance is lost because of a lateral posture threat (*52*) or save more energy when an external stabilizer aids gait (*34*). This suggests that the assistance may have caused more balance-related efforts from participants (*20*, *21*); however, when assistance was given in a timely manner (the MS), the participants could receive the metabolic benefit, overcoming the increased balance-related effort.

We aimed to understand the effects of hip abduction assistance. For an initial step, we investigated the effect of assistance timing as other parameters (such as force magnitude and assistance duration) were kept constant. The magnitude of force and assistance duration could substantially influence the gaits (*10*, *11*). In addition, all the powered profiles tended to have lower dynamic stability compared with the normal walking condition, meaning that the hip abduction assistance can be further improved. Applying a moderate assistance profile by transmitting a lower force or slower velocity would have helped the participants walk more steadily. In conclusion, we developed hip abduction assistance profiles based on the peak timing of biological moment and power. Given assistance, we observed that users responded differently. Several studies have shown that such interparticipant variability can be reduced when the participants adapt more to robot assistance (*12*, *46*, *53*) and when a wearable robot is optimized for each user (*11*, *19*, *27*, *54*–*57*). By following the progress of the explored wearable robotics studies focused on assisting other joints or on the sagittal plane, we expect that the effectiveness of hip abduction assistance can be improved.

MATERIALS AND METHODS

Experimental protocol

The experiments were conducted with 10 healthy participants (10 males, age: 25.50 ± 1.69 years, height: 1.75 ± 0.06 m, mass: 70.8 ± 10.19 kg, mean ± SD). The experimental protocol is represented in Fig. 1. At the beginning of the experiment, while the participants stood in a quiet posture, standing metabolism and static posture recordings were collected for 5 min. Thereafter, the participants walked on a customized treadmill (KIMSPORTS, South Korea) at the constant speed of 1.38 m s^{-1} for 6 min. They wore an exosuit and proceeded with the training section called enforced exploration.

Enforced exploration was conducted to allow the participants to adapt to robot assistance. During enforced exploration, the participants walked with an abnormal gait posture, including upper body leaning to the left, right, forward, and backward; walking with a higher or lower frequency; and taking wider or narrower steps. The participants were informed about these movements before the session. When the enforced exploration period began, robot assistance was applied for 12 min. At the time, four assistance profiles were applied for 3 min each and in a random order. The participants walked freely during the first 1 min and then walked with the help of verbal instructions during the last 2 min. The instructor requested the participants to change their gait posture every 15 s.

After the enforced exploration, each assistance profile was applied for 6 min. The order of the four conditions with each assistance profile was randomized. A 5-min relaxation gap was allowed between the conditions. The experimental protocol was approved by the Chung-ang University Institutional Review Board, and the participants provided informed consent.

Actuator specification

In human gait, biological torque is usually generated at the level of about 1 N•m per kg at the hip joint in the frontal plane (*25*, *58*). Among the hip assistance robots, a wearable robot providing biological improvement can assist the wearer by offering about 18 to 30% of biological torque (*11*, *19*, *30*, *54*). Because the moment arm of the hip joint in the frontal plane is shorter than the one of the sagittal plane, reaching the moment level of a conventional wearable robot requires a greater force and may cause suit deformation or user discomfort. Thus, we chose actuation parts, including the motor and gear, such that the system could generate more than 10% of the biological torque, a moment level slightly lower than that of other wearable robots. The selected systems were as follows (fig. S3): motor (EC 4 pole, 200 W, Maxon, Switzerland) with a maximum speed of 16,000 rpm and a stall torque of 3.43 Nm; planetary gear (Planetary Gearhead GP 32 HP, Maxon, Switzerland) with a ratio of 79:1; and pulley with a circumference of 40 mm attached to the front of the gear to transmit power to the cable. Through this setup, the peak torque generated at the final stage of the motor was 10.83 N•m, which could offer about 14% of the biological torque based on the 70-kg body weight of the participant. The encoder (1024 counts per revolution, Encoder 16 EASY, Maxon, Switzerland) was attached to the back of the motor. This measured the state of the motor, including the position, velocity, and current.

Soft exosuit

For force transmission through the cable to assist hip abduction, a lateral torque should be generated against the hip joint. Considering

this principle, the anchoring point and the shape of the suit were designed accordingly (Fig. 7). The suit was divided into the thigh part and the waist belt (fig. S4). The anchoring point was located on the lateral side of the thigh part and waist belt. To transmit torque in the lateral direction, these two anchoring points were manufactured such that they were placed in a straight line with the vertical direction of the body in the standing position. Three buckles (COBRA ProStyle – Fixed, AustriAlpin, Austria) were attached to each side of the waist belt so that people with different body shapes could wear the exosuit. The load cell was connected at the anchoring point of the thigh part using a pin.

To minimize the deformation caused by assistance, each part should be firmly fixed to the body. Thus, in this study, X-shaped suspenders were used to fix the upper part of the body. The strap started from the front top of the waist belt and passed through the shoulder. The end of the strap was located above the anchoring point of the waist belt. To prevent the thigh part from sliding down while walking, two bands per leg were released from the waist belt and were connected to the thigh part through a buckle. In addition, a foam-type guard was attached under the waist anchoring point to prevent the skin from being rubbed or pressed by the cable or other mechanical parts.

Sensors and control

A PC ran all of the systems through LabVIEW and was connected to a programmable automation controller [compactRIO-9040(cRIO), National Instrument, USA]. Three inertial measurement units (IMU) (MTi-630, XSENS, Netherlands) were used to measure the wearer's motions. These were attached to the top of each foot and the front of the right thigh. The sensors were connected to a cRIO through controller area network (CAN) communication. A CAN module (NI-9853, National Instruments, USA) was also used. Load cell sensors (LSB 205, Futek, USA) were used to measure the force. The sensors were fixed at the anchoring point of the thigh part using a pin. A multifunction I/O module (NI-9381 and NI-9923, National Instruments, USA) received data from the load cells via an analog connection and was connected to the cRIO. In addition, the cRIO was connected through the Ethernet for Control Automation Technology (EtherCAT) communication with a motor driver (Gold Solo Twitter 10/100, Elmo Motion Control, Israel), which drove the motor and monitored the status of the motors.

Gait event detection

In this study, an IMU-based gait detection algorithm was designed to deliver a consistent assistance profile over the gait cycle. The gait cycle percentage was estimated through the angular velocity in the sagittal plane of the IMU sensor attached to the top of each foot. We set the zero-crossing point in the negative direction as an HS (*59*). The current gait cycle percentage was obtained by dividing the time increment from the previous detected point by the stride period. We used the average of the three most recent stride times as the denominator. A simple real-time lowpass filter (6-Hz cutoff frequency, second order) was applied to the IMU signals for algorithm usage.

PD-type iterative learning controller

To create a proper assistance profile, we introduced the proportional derivative (PD)–type iterative learning controller, typically used when a system runs repetitive tasks (*22*). It can use the knowledge of prior iterations to reduce the overall error by correcting the next iteration. The reference output $y_d(t)$ is an invariant over the iteration, whereas $u(t)$ is updated by the learning rule. The update rules of the PD-type ILC can be described as follows:

$$u^{k+1}(t) = u^k(t) + K_\mathrm{p}\ e^k(t+1) + K_\mathrm{D}\ \Delta e^k(t+1) \tag{1}$$

where $u^k(t)$ is the state input at the kth iteration, $e^k(t)$ is the tracking error at the kth iteration, and $\Delta e^k(t)$ is the error difference between the nearest iterations.

$$e^k(t) = y_d(t) - y^k(t),\ \ \Delta e^k(t) = e^k(t) - e^{k-1}(t) \tag{2}$$

where K_p and K_D are the proportional and derivative gains of the system, respectively.

Measurement and data processing

The respiratory data were collected through a portable respiratory analyzer (K5, COSMED, Italy), and the metabolic rate was calculated using the Brockway equation (*60*), by considering the oxygen and carbon dioxide rates in the region during the last 2 min for each condition. Insole-type pressure sensors (Xsensor, XSENSOR Technology Corporation, Canada) were mounted inside the shoes to gather pressure data. The kinematics data were collected using a motion capture system with eight cameras (Nexus2, VICON, USA; 6-T-series and 2-Vantage, VICON, USA). Furthermore, 29 markers were attached to the participant's anatomical points based on the plug-in-gait model.

The MoS is a method that can assess dynamic walking stability (*36*, *51*) and is defined as the minimum distance between the base of support (BoS) and XCoM. The XCoM is a variable that considers the position of the CoM with its velocity.

$$\mathrm{XCoM} = P + \sqrt{\frac{l}{g}}V \tag{3}$$

$$\mathrm{MoS_{ML}} = \mathrm{BoS_{ML}} - \mathrm{XCoM_{ML}} \tag{4}$$

where P is the position of the CoM and V is the velocity of the CoM, which can be calculated by differentiating P. l is the leg length of the inverted pendulum model, defined as the maximum vertical distance between the sacrum marker and the ground. g is the gravitational acceleration (9.81 m/s^2). The lateral border of the BoS is defined as the lateral position of the fifth metatarsal marker. Changes in balance-related effort can be judged using the average step width and its variability (*22*, *38*–*40*). Adjusting the foot placement is one such strategy for controlling balance during walking (*22*, *37*, *61*). When a disturbance is applied during walking, people usually increase their step width variability. In this study, the average step width and step width variability were calculated using the marker data at midstance. The midstance is defined at the moment the sacrum marker goes through the foot center, which is the midpoint of the heel marker and toe marker in the forward direction. The step width is the mean distance between the center of both feet in the mediolateral direction, and the step width variability is the SD of the average step width. The balance-related effort is also reflected through the variability of the CoP. For example, the variability of the CoP tends to increase in chronic ankle instability patients (*41*) and high-heel gait with muscle fatigue (*62*). The variability of the CoP is defined as the SD of the mediolateral location of the CoP within the stance phase.

In this study, we also measured the spatiotemporal parameters, including the stride length, cadence, stance time, swing time, and double stance time. The stride length is defined as the distance between two heel markers at the moment of HS. Cadence is the reciprocal of stride time, which is the time difference from the prior HS to the current moment of HS. The stance time and swing time are the time differences from HS to toe-off and from toe-off to HS, respectively. The double stance time is the ratio of the time both feet are in contact with the ground to the strike time. All the parameters were processed for the last 120 strides and averaged across the participants using MATLAB (MathWorks, USA) and Visual3D (C-motion, USA).

Statistical analysis

We conducted a statistical analysis using SPSS (IBM SPSS statistics 26, USA). The normality of the data was analyzed via the Shapiro-Wilk test. When the data were normally distributed, we performed repeated-measures ANOVA (random effect: participant; fixed effect: assistance timing); however, when the data were not normally distributed, we conducted the Friedman test. We used paired *t* tests with a Šidák-Holm correction for multiple comparisons between four powered conditions. If the data were not normally distributed, then we used the Dunn-Bonferroni test for multiple comparisons between four powered conditions (*63*). If any statistical difference appeared, then we compared the best condition (showing minimum metabolic rate) with the normal walking condition using a paired *t* test. All analyses were conducted with a significance level of $\alpha < 0.05$.

Supplementary Materials

This PDF file includes:
Supplementary Text
Figs. S1 to S11
Tables S1 to S5
References (*64*, *65*)

Other Supplementary Material for this manuscript includes the following:
Data file S1
MDAR Reproducibility Checklist

REFERENCES AND NOTES

1. M. S. Johansson, M. Korshøj, P. Schnohr, J. L. Marott, E. I. B. Prescott, K. Søgaard, A. Holtermann, Time spent cycling, walking, running, standing and sedentary: A cross-sectional analysis of accelerometer-data from 1670 adults in the Copenhagen City Heart Study: Physical behaviours among 1670 Copenhageners. *BMC Public Health* **19**, 1–13 (2019).
2. T. Althoff, R. Sosič, J. L. Hicks, A. C. King, S. L. Delp, J. Leskovec, Large-scale physical activity data reveal worldwide activity inequality. *Nature* **547**, 336–339 (2017).
3. C. Tudor-Locke, S. A. Ham, C. A. Macera, B. E. Ainsworth, K. A. Kirtland, J. P. Reis, C. D. Kimsey, Descriptive epidemiology of pedometer-determined physical activity. *Med. Sci. Sports Exerc.* **36**, 1567–1573 (2004).
4. Y. Schutz, S. Weinsier, P. Terrier, D. Durrer, A new accelerometric method to assess the daily walking practice. *Int. J. Obes. (Lond)* **26**, 111–118 (2002).
5. J. A. Levine, S. J. Schleusner, M. D. Jensen, Energy expenditure of nonexercise activity. *Am. J. Clin. Nutr.* **72**, 1451–1454 (2000).
6. G. S. Sawicki, O. N. Beck, I. Kang, A. J. Young, The exoskeleton expansion: Improving walking and running economy. *J. Neuroeng. Rehabil.* **17**, 25 (2020).
7. P. Malcolm, W. Derave, S. Galle, D. De Clercq, A simple exoskeleton that assists plantarflexion can reduce the metabolic cost of human walking. *PLOS ONE* **8**, e56137 (2013).
8. P. Malcolm, R. E. Quesada, J. M. Caputo, S. H. Collins, The influence of push-off timing in a robotic ankle-foot prosthesis on the energetics and mechanics of walking. *J. Neuroeng. Rehabil.* **12**, 21 (2015).
9. Y. Ding, F. A. Panizzolo, C. Siviy, P. Malcolm, I. Galiana, K. G. Holt, C. J. Walsh, Effect of timing of hip extension assistance during loaded walking with a soft exosuit. *J. Neuroeng. Rehabil.* **13**, 87 (2016).
10. B. T. Quinlivan, S. Lee, P. Malcolm, D. M. Rossi, M. Grimmer, C. Siviy, N. Karavas, D. Wagner, A. Asbeck, I. Galiana, C. J. Walsh, Assistance magnitude versus metabolic cost reductions for a tethered multiarticular soft exosuit. *Sci. Robot.* **2**, eaah4416 (2017).
11. Y. Ding, M. Kim, S. Kuindersma, C. J. Walsh, Human-in-the-loop optimization of hip assistance with a soft exosuit during walking. *Sci. Robot.* **3**, eaar5438 (2018).
12. K. L. Poggensee, S. H. Collins, How adaptation, training, and customization contribute to benefits from exoskeleton assistance. *Sci Robot.* **6**, eabf1078 (2021).
13. K. A. Witte, P. Fiers, A. L. Sheets-Singer, S. H. Collins, Improving the energy economy of human running with powered and unpowered ankle exoskeleton assistance. *Sci. Robot.* **5**, eaay9108 (2020).
14. G. Lee, J. Kim, F. A. Panizzolo, Y. M. Zhou, L. M. Baker, I. Galiana, P. Malcolm, C. J. Walsh, Reducing the metabolic cost of running with a tethered soft exosuit. *Sci. Robot.* **2**, eaan6708 (2017).
15. J. Kim, G. Lee, R. Heimgartner, D. Arumukhom Revi, N. Karavas, D. Nathanson, I. Galiana, A. Eckert-Erdheim, P. Murphy, D. Perry, N. Menard, D. K. Choe, P. Malcolm, C. J. Walsh, Reducing the metabolic rate of walking and running with a versatile, portable exosuit. *Science* **365**, 668–672 (2019).
16. R. Baud, A. R. Manzoori, A. Ijspeert, M. Bouri, Review of control strategies for lower-limb exoskeletons to assist gait. *J. Neuroeng. Rehabil.* **18**, 119 (2021).
17. M. Wehner, B. Quinlivan, P. M. Aubin, E. Martinez-Villalpando, M. Baumann, L. Stirling, K. Holt, R. Wood, C. Walsh, A lightweight soft exosuit for gait assistance, in *2013 IEEE International Conference on Robotics and Automation*, Karlsruhe, Germany, 6 to 10 May 2013 (IEEE, 2013), pp. 3362–3369.
18. S. H. Collins, M. Bruce Wiggin, G. S. Sawicki, Reducing the energy cost of human walking using an unpowered exoskeleton. *Nature* **522**, 212–215 (2015).
19. G. M. Bryan, P. W. Franks, S. Song, A. S. Voloshina, R. Reyes, M. P. O'Donovan, K. N. Gregorczyk, S. H. Collins, Optimized hip–knee–ankle exoskeleton assistance at a range of walking speeds. *J. Neuroeng. Rehabil.* **18**, 152 (2021).
20. M. Kim, S. H. Collins, Once-per-step control of ankle-foot prosthesis push-off work reduces effort associated with balance during walking. *J. Neuroeng. Rehabil.* **12**, 43 (2015).
21. M. Kim, S. H. Collins, Once-per-step control of ankle push-off work improves balance in a three-dimensional simulation of bipedal walking. *IEEE Trans. Robot.* **33**, 406–418 (2017).
22. H. Reimann, T. Fettrow, J. J. Jeka, Strategies for the control of balance during locomotion. *Kinesiology Rev.* **7**, 18–25 (2018).
23. L. G. Brough, G. K. Klute, R. R. Neptune, Biomechanical response to mediolateral foot-placement perturbations during walking. *J. Biomech.* **116**, 110213 (2021).
24. J. Perry, *Gait Analysis : Normal and Pathological Function* (Slack Incorporated, ed. 2, 2010), p. 551.
25. D. A. Winter, *Biomechanics and Motor Control of Human Movement* (John Wiley & Sons Inc., 2009), p. 277.
26. C. L. Dembia, A. Silder, T. K. Uchida, J. L. Hicks, S. L. Delp, Simulating ideal assistive devices to reduce the metabolic cost of walking with heavy loads. *PLOS ONE* **12**, e0180320 (2017).
27. J. Zhang, P. Fiers, K. A. Witte, R. W. Jackson, K. L. Poggensee, C. G. Atkeson, S. H. Collins, Human-in-the-loop optimization of exoskeleton assistance during walking. *Science* **356**, 1280–1284 (2017).
28. T. Zhang, M. Tran, H. Huang, Design and experimental verification of hip exoskeleton with balance capacities for walking assistance. *IEEE ASME Trans.Mechatron.* **23**, 274–285 (2018).
29. V. L. Chiu, M. Raitor, S. H. Collins, Design of a hip exoskeleton with actuation in frontal and sagittal planes. *IEEE Trans. Med. Robot. Bionics* **3**, 773–782 (2021).
30. H. D. Yang, M. Cooper, A. Eckert-Erdheim, D. Orzel, C. J. Walsh, A soft exosuit assisting hip abduction for knee adduction moment reduction during walking. *IEEE Robot. Autom. Lett.* **7**, 7439–7446 (2022).
31. A. D. Kuo, Stabilization of lateral motion in passive dynamic walking. *Int. J. Rob. Res.* **18**, 917–930 (1999).
32. C. E. Bauby, A. D. Kuo, Active control of lateral balance in human walking. *J. Biomech.* **33**, 1433–1440 (2000).
33. Y. Wang, M. Srinivasan, Stepping in the direction of the fall: The next foot placement can be predicted from current upper body state in steady-state walking. *Biol. Lett.* **10**, 20140405 (2014).
34. J. C. Dean, N. B. Alexander, A. D. Kuo, The effect of lateral stabilization on walking in young and old adults. *IEEE Trans. Biomed. Eng.* **54**, 1919–1926 (2007).
35. M. Vlutters, E. H. F. van Asseldonk, H. van der Kooij, Lower extremity joint-level responses to pelvis perturbation during human walking. *Sci. Rep.* **8**, 14621 (2018).

36. A. L. Hof, M. G. J. Gazendam, W. E. Sinke, The condition for dynamic stability. *J. Biomech.* **38**, 1–8 (2005).
37. M. A. Townsend, Biped gait stabilization via foot placement. *J. Biomech.* **18**, 21–38 (1985).
38. T. M. Owings, M. D. Grabiner, Step width variability, but not step length variability or step time variability, discriminates gait of healthy young and older adults during treadmill locomotion. *J. Biomech.* **37**, 935–938 (2004).
39. S. M. O'Connor, H. Z. Xu, A. D. Kuo, Energetic cost of walking with increased step variability. *Gait Posture* **36**, 102–107 (2012).
40. J. A. Perry, M. Srinivasan, Walking with wider steps changes foot placement control, increases kinematic variability and does not improve linear stability. *R. Soc. Open Sci.* **4**, 160627 (2017).
41. R. M. Koldenhoven, M. A. Feger, J. J. Fraser, J. Hertel, Variability in center of pressure position and muscle activation during walking with chronic ankle instability. *J. Electromyogr. Kinesiol.* **38**, 155–161 (2018).
42. H. Herr, M. Popovic, Angular momentum in human walking. *J. Exp. Biol.* **211**, 467–481 (2008).
43. J. K. Leestma, P. R. Golyski, C. R. Smith, G. S. Sawicki, A. J. Young, G. W. Woodruff, Linking whole-body angular momentum and step placement during perturbed human walking. *J. Exp. Biol.* **226**, jeb244760 (2023).
44. C. Liu, L. De Macedo, J. M. Finley, Conservation of reactive stabilization strategies in the presence of step length asymmetries during walking. *Front. Hum. Neurosci.* **12**, 251 (2018).
45. J. C. Selinger, S. M. O'Connor, J. D. Wong, J. M. Donelan, Humans can continuously optimize energetic cost during walking. *Curr. Biol.* **25**, 2452–2456 (2015).
46. M. Kim, H. Jeong, P. Kantharaju, D. Yoo, M. Jacobson, D. Shin, C. Han, J. L. Patton, Visual guidance can help with the use of a robotic exoskeleton during human walking. *Sci. Rep.* **12**, 3881 (2022).
47. G. S. Sawicki, D. P. Ferris, Powered ankle exoskeletons reveal the metabolic cost of plantar flexor mechanical work during walking with longer steps at constant step frequency. *J. Exp. Biol.* **212**, 21–31 (2009).
48. L. M. Mooney, E. J. Rouse, H. M. Herr, Autonomous exoskeleton reduces metabolic cost of human walking during load carriage. *J. Neuroeng. Rehabil.* **11**, 80 (2014).
49. S. Galle, P. Malcolm, S. H. Collins, D. De Clercq, Reducing the metabolic cost of walking with an ankle exoskeleton: Interaction between actuation timing and power. *J. Neuroeng. Rehabil.* **14**, 35 (2017).
50. L. Hak, H. Houdijk, P. van der Wurff, M. R. Prins, A. Mert, P. J. Beek, J. H. van Dieën, Stepping strategies used by post-stroke individuals to maintain margins of stability during walking. *Clin. Biomech.* **28**, 1041–1048 (2013).
51. F. Watson, P. C. Fino, M. Thornton, C. Heracleous, R. Loureiro, J. J. H. Leong, Use of the margin of stability to quantify stability in pathologic gait—A qualitative systematic review. *BMC Musculoskelet. Disord.* **22**, 597 (2021).
52. T. IJmker, C. J. Lamoth, H. Houdijk, L. H. van der Woude, P. J. Beek, Postural threat during walking: Effects on energy cost and accompanying gait changes. *J. Neuroeng. Rehabil.* **11**, 71 (2014).
53. F. A. Panizzolo, G. M. Freisinger, N. Karavas, A. M. Eckert-Erdheim, C. Siviy, A. Long, R. A. Zifchock, M. E. LaFiandra, C. J. Walsh, Metabolic cost adaptations during training with a soft exosuit assisting the hip joint. *Sci. Rep.* **9**, 9779 (2019).
54. S. Lee, J. Kim, L. Baker, A. Long, N. Karavas, N. Menard, I. Galiana, C. J. Walsh, Autonomous multi-joint soft exosuit with augmentation-power-based control parameter tuning reduces energy cost of loaded walking. *J. Neuroeng. Rehabil.* **15**, 66 (2018).
55. P. Kantharaju, H. Jeong, S. Ramadurai, M. Jacobson, H. Jeong, M. Kim, Reducing squat physical effort using personalized assistance from an ankle exoskeleton. *IEEE Trans. Neural Syst. Rehabil. Eng.* **30**, 1786–1795 (2022).
56. M. Jacobson, P. Kantharaju, H. Jeong, J.-K. Ryu, J.-J. Park, H.-J. Chung, M. Kim, Foot contact forces can be used to personalize a wearable robot during human walking. *Sci. Rep.* **12**, 10947 (2022).
57. T.-C. Wen, M. Jacobson, X. Zhou, H.-J. Chung, M. Kim, The personalization of stiffness for an ankle-foot prosthesis emulator using human-in-the-loop optimization, in *2020 IEEE/RSJ International Conference on Intelligent Robots and Systems (IROS)*, Las Vegas, NV, 24 October 2020 to 24 January 2021 (IEEE, 2020), pp. 3431–3436.
58. C. A. Fukuchi, R. K. Fukuchi, M. Duarte, A public dataset of overground and treadmill walking kinematics and kinetics in healthy individuals. *PeerJ.* **6**, e4640 (2018).
59. J. C. Perez-Ibarra, A. A. G. Siqueira, H. I. Krebs, Real-time identification of gait events in impaired subjects using a single-IMU foot-mounted device. *IEEE Sens. J.* **20**, 2616–2624 (2020).
60. J. M. Brockway, Derivation of formulae used to calculate energy expenditure in man. *Hum. Nutr. Clin. Nutr.* **41**, 463–471 (1987).
61. B. L. Rankin, S. K. Buffo, J. C. Dean, A neuromechanical strategy for mediolateral foot placement in walking humans. *J. Neurophysiol.* **112**, 374–383 (2014).
62. A. Gefen, M. Megido-Ravid, Y. Itzchak, M. Arcan, Analysis of muscular fatigue and foot stability during high-heeled gait. *Gait Posture* **15**, 56–63 (2002).
63. O. J. Dunn, Multiple Comparisons Using Rank Sums. *Dent. Tech.* **6**, 241–252 (1964).
64. M. W. Whittle, *An Introduction to Gait Analysis* (Butterworth-Heinemann, 2014.).
65. P. R. Golyski, E. Vazquez, J. K. Leestma, G. S. Sawicki, Onset timing of treadmill belt perturbations influences stability during walking. *J. Biomech.* **130**, 110800 (2022).

Acknowledgments

Funding: This work was supported by the Industrial Strategic Technology Development Program (no. 20007058), funded by the Ministry of Trade, Industry, & Energy (MOTIE, Korea), MSIT (Ministry of Science, ICT), Korea, under the High-Potential Individuals Global Training Program) (2021-0-01538) supervised by the IITP (Institute for Information & Communications Technology Planning & Evaluation); Basic Science Research Program through the National Research Foundation of Korea (NRF), funded by the Ministry of Education (no. 2021R1A4A3030268); R&D Program for Forest Science Technology (no. 2021364B10-2123-BD01) provided by the Korea Forest Service (Korea Forestry Promotion Institute); and Korea Medical Device Development Fund grant funded by the Korea government (the Ministry of Science and ICT, the Ministry of Trade, Industry and Energy, the Ministry of Health & Welfare, the Ministry of Food and Drug Safety) (RS-2022-00140621). **Author contributions:** Conceptualization: J.P., M.K., and G.L. System design: J.P., J.M., J.R., and S.Y. System fabrication: J.P., J.M., J.R., and S.Y. Exosuit design: J.P. and S.P. Exosuit fabrication: S.P. Conducting experiment: J.P., K.N., J.Y., and A.N. Analyzing and interpreting data: J.P., A.N., W.N., S.R., M.K., and G.L. Visualization: J.P., J.M., J.R., S.P., M.K., and G.L. Funding acquisition: M.K. and G.L. Project administration: M.K. and G.L. Supervision: M.K. and G.L. Writing—original draft: J.P., M.K., and G.L. Writing—review & editing: J.P., M.K., and G.L. **Competing interests:** The authors declare that they have no competing interests. **Data and materials availability:** All data are available in the main text, the Supplementary Materials, or at the following link: https://doi.org/10.5281/zenodo.8367402.

Submitted 5 August 2022
Accepted 27 September 2023
Published 25 October 2023
10.1126/scirobotics.ade0876

Science Robotics

Effect of hip abduction assistance on metabolic cost and balance during human walking

Juneil Park, Kimoon Nam, Juseok Yun, JunYoung Moon, JaeWook Ryu, Sungjin Park, Seungtae Yang, Alireza Nasirzadeh, Woochul Nam, Sruthi Ramadurai, Myunghee Kim, and Giuk Lee

Sci. Robot. **8** (83), eade0876. DOI: 10.1126/scirobotics.ade0876

Science Robotics (ISSN 2470-9476) is published by the American Association for the Advancement of Science. 1200 New York Avenue NW, Washington, DC 20005. The title *Science Robotics* is a registered trademark of AAAS.